Magnetization, specific heat, ^{17}O NMR, and ^{237}Np Mössbauer study of $U_{0.15}Np_{0.85}O_2$

Laura Martel,[1,*] Amir Hen,[1,2] Yo Tokunaga,[3] François Kinnart,[1] Nicola Magnani,[1] Eric Colineau,[1] Jean-Christophe Griveau,[1] and Roberto Caciuffo[1]

[1]*European Commission, Joint Research Centre (JRC), Directorate for Nuclear Safety and Security, Postfach 2340, D-76125 Karlsruhe, Germany*

[2]*ESRF, European Synchrotron Radiation Facility, 71 Av. des Martyrs, Grenoble Cedex 09, France*

[3]*Advanced Science Research Centre, Japan Atomic Energy Agency, Tokai, Naka-gun, Ibaraki 319-1195, Japan*

(Received 5 February 2018; revised manuscript received 15 May 2018; published 5 July 2018)

We report a study of the magnetic and electronic properties of the $U_{0.15}Np_{0.85}O_2$ solid solution, based on dc- and ac magnetization, ^{237}Np Mössbauer spectroscopy, ^{17}O nuclear magnetic resonance, and specific heat measurements. The compound orders antiferromagnetically at $T_N = 17$ K. The different techniques reveal the complexity of this system with: (*i*) a spatial distribution of ordered moments, (*ii*) a small Np ordered moment ($\mu_{Np} = 0.3\ \mu_B$), and (*iii*) an additional specific heat anomaly at 7.4 K, with a residual value at very low temperature and a reduced magnetic entropy. The results are compared to the end members of the series, UO_2 and NpO_2, as well as to the other solid solutions previously reported in this system. We discuss how the properties of $U_{0.15}Np_{0.85}O_2$ add input to the trend previously reported for the series in view of the models that have been proposed.

DOI: 10.1103/PhysRevB.98.014410

I. INTRODUCTION

The $U_{1-x}Np_xO_2$ solid solutions are considered as potential fuels and targets for the transmutation of the minor actinide in fast neutron reactors [1,2]. A great interest has been devoted in the last thirty years for the understanding of their very unique and intriguing magnetic properties. The two end members of this series exhibit different types of order: while UO_2 is a type-I antiferromagnet ($T_N = 30.8$ K) [3], no ordered dipolar magnetic moment was found for NpO_2 by neutron [4,5] and Mössbauer spectroscopy [6–8], despite the evidence that a λ-type peak around $T_0 = 26$ K is present in the specific heat measurements. In fact, the primary order parameter in this case is a higher-order magnetic multipole [9–12], namely a rank-5 triakontadipole [13,14]. Both UO_2 and NpO_2 also display antiferroquadrupolar (AFQ) order as a secondary order parameter [12,15,16], with a transverse 3-*k* structure in UO_2 (AFQ-T) and a longitudinal 3 *k* in NpO_2 (AFQ-L). Coexisting dipolar and quadrupolar order is also observed in the intermediate $U_{1-x}Np_xO_2$ mixed oxides, but the or dering temperature does not follow a linear Vegard-type law and exhibits a minimum around $x \sim 0.6$–0.8 [17]; the substitution of U by Np reduces the importance of dipolar exchange interactions, eventually making them irrelevant once the system enters the multipolar-ordered state.

The first analyses made on mixed oxides were done using magnetic susceptibility and Mössbauer spectroscopy for compositions $x = 0.15$, 0.25, 0.5, and 0.75 [18]. Independently, three compositions were studied by neutron diffraction ($x =$ 0.25 [19], 0.5 [20], and 0.75 [19]) and one by resonant x-ray scattering and specific heat ($x = 0.75$) [17]. Wilkins *et al.* [3] focused on the AFQ ordering and studied three additional compositions ($x = 0.05$, 0.45, and 0.95), suggesting the presence of three different regions: AFQ-T for $0 \leqslant x \leqslant 0.3$, short-range quadrupolar ordering for $0.3 < x \leqslant 0.8$, and AFQ-L for $x > 0.8$, the intermediate phase resulting from the competition between Np-Np triakontadipolar interactions and U-Np and U-U dipolar interactions.

In this study, we investigated specifically the magnetic and electronic properties of the $U_{0.15}Np_{0.85}O_2$ compound—-which is located close to the border between the short-range and AFQ-L regions—-using magnetic susceptibility, ^{17}O NMR, ^{237}Np Mössbauer spectroscopy, and specific heat.

II. EXPERIMENTAL

The powder sample was synthesized using the sol-gel method and then enriched in ^{17}O using the gas-exchange technique. The crystallinity and homogeneity were checked using x-ray diffraction and the lattice parameter ($a = 5.440$ (1) Å) was found consistent with Vegard's law. More precise details on the synthesis and full characterization of the sample using high-resolution solid-state NMR and x-ray absorption near edge structure (XANES) are available in Ref. [21]. Due to the high radiotoxicity of the sample, the powders (about 150 mg) used for magnetization and NMR studies were encapsulated in double-Plexiglas containers and fixed with a Stycast® 1266 epoxy resin.

dc magnetization was performed using a Quantum Design MPMS-7 device in the temperature range 2–300 K with four different applied magnetic field values: $\mu_0 H = 0$, 1, 5, and 7 T. ac magnetic susceptibility measurements were made with a PPMS-14 at $\mu_0 H = 0$ T with frequencies ranging from 63 to 9887 Hz.

Heat capacity experiments were performed by a relaxation technique in the temperature range of 2.5–300 K in magnetic fields up to 9 T using a Quantum Design PPMS-9 device.

*laura.martel@ec.europa.eu

The ^{237}Np Mössbauer measurements were performed in transmission geometry on a powder absorber with a thickness of 140 mg cm^{-2} of Np. The Mössbauer source (∼108 mCi of ^{241}Am metal) was kept at 4.2 K, while the temperature of the absorber was varied from 4.2 to 40 K in discrete steps. The spectra were recorded with a sinusoidal drive system using conventional methods. No magnetic field was applied. The $NpAl_2$ standard was used as a reference to calibrate the velocity scale ($B_{hf} = 330$ T at 4.2 K).

The ^{17}O NMR experiments were performed on a PPMS-9T from Quantum Design equipped with a THAMWAY PROTII NMR spectrometer. A specially designed NMR probe dedicated to the low-temperature study of radioactive materials was used.

III. EXPERIMENTAL RESULTS

A. Magnetic measurements

The temperature dependence of the dc magnetic susceptibility (M/H) and its inverse (H/M) are presented in Fig. 1. As no difference was observed between field-cooled and zero-field-cooled behaviors, only the field-cooled curves are shown. A clear magnetic anomaly is observed at $T_N = 17$ K. This transition is very robust in applied magnetic fields and the Néel temperature is not affected up to the maximum field accessible with our superconducting quantum interference device (7 T) (top inset in Fig. 1). The magnetization is also far from saturation and no metamagnetic transitions occur within the studied field and temperature range (right inset, Fig. 1).

Above ∼40 K, the magnetic susceptibility can be fitted with a modified Curie-Weiss law $\chi = \chi_0 + \frac{N\mu_{eff}^2\mu_B^2}{3k_B}\frac{1}{T-\theta_P}$ (Fig. 1). We obtained a temperature-independent term $\chi_0 = 3 \cdot 10^{-4}$ emu/mol which includes the core-electron diamagnetism, the Pauli paramagnetism, and Van Vleck contribution. A paramagnetic Curie temperature of $\theta_P = -94.7$ K was determined. The negative θ_P value indicates the presence of antiferromagnetic interactions. Finally, an effective moment $\mu_{eff} = 2.73\mu_B$ was calculated. This value is reduced compared to the free-ion values ($\mu_{eff} = 3.58\mu_B$ for U^{4+} and $\mu_{eff} = 3.62\mu_B$ for Np^{4+} in Russell-Saunders coupling [20]). While the μ_{eff} of 3.6 μ_B published for UO_2 [22] is in good agreement with the free-ion model, a μ_{eff} with a reduced value of $2.95\mu_B$ was found for NpO_2 [42]. This behavior will be examined in more detail in Sec. IV.

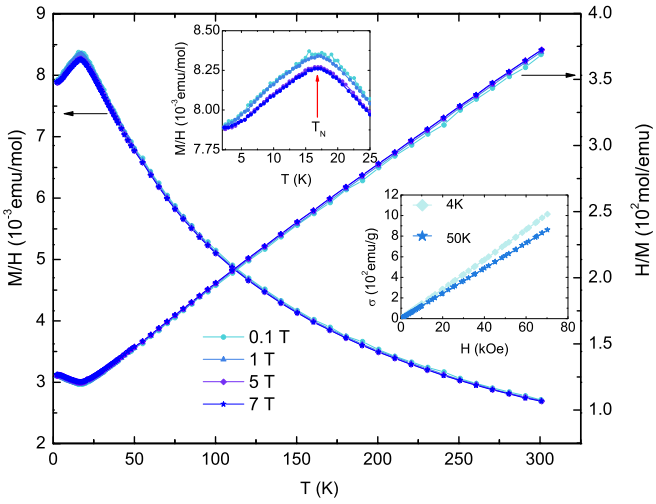

FIG. 1. Temperature (T) dependence of the magnetic susceptibility M/H and its inverse H/M, measured in four different magnetic fields: $\mu_0 H = 0.1, 1, 5$, and 7 T. The straight line is a fit to the modified Curie-Weiss law. The inset on the top is a zoom on the magnetic transition zone at different magnetic fields. The other inset (right) represents magnetization (σ) versus magnetic field taken at several temperatures.

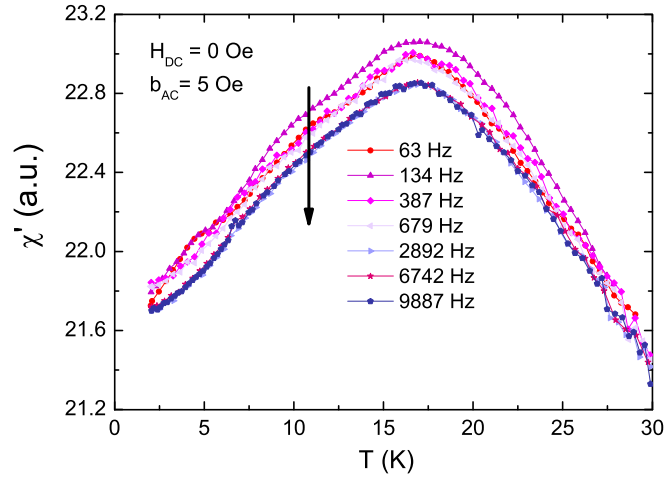

FIG. 2. ac magnetic susceptibility (χ') in arbitrary unit (a.u.) versus temperature acquired at different frequencies under a magnetic field of $H = 0$ T and an applied ac magnetic field (b_{ac}) of 5 Oe. The arrow indicates a slight decrease of the peak intensity with frequency.

We also found relevant to record the ac magnetic susceptibility and present it in Fig. 2. As the curve is similar to the dc susceptibility, it confirms the onset of magnetic ordering at T_N. The absence of frequency dependence suggests the absence of short-range ordering.

B. Oxygen-17 NMR

Figure 3 presents the temperature dependence of the static ^{17}O field-sweep NMR spectrum. At 20 K, above the ordering temperature, the spectrum is characterized by a single main peak with a weak shoulder at lower fields. The main peak corresponds to the central transition and is due to the overlapping of the $O(Np)_y(U)_{4-y}$ different local environments due to the substitution of Np by the U cation as previously detected by high-resolution ^{17}O solid-state NMR at room temperature [21]. The weak shoulder at lower field was already visible at room temperature and does not correspond to the central transition. Instead, it was previously attributed to the spinning sidebands by high-resolution NMR [21–27]. We want to stress that a less visible shoulder is also detected at higher field compared to the main peak (not shown). Thus, ^{17}O high-resolution solid-state NMR coupled with x-ray diffraction (XRD) and XANES confirms the purity of this sample. The single peak detected in static conditions was also observed for UO_2 and NpO_2 in the paramagnetic state [28,29]. Below 17 K, there is a rapid increase of the line broadening as shown in Fig. 3.

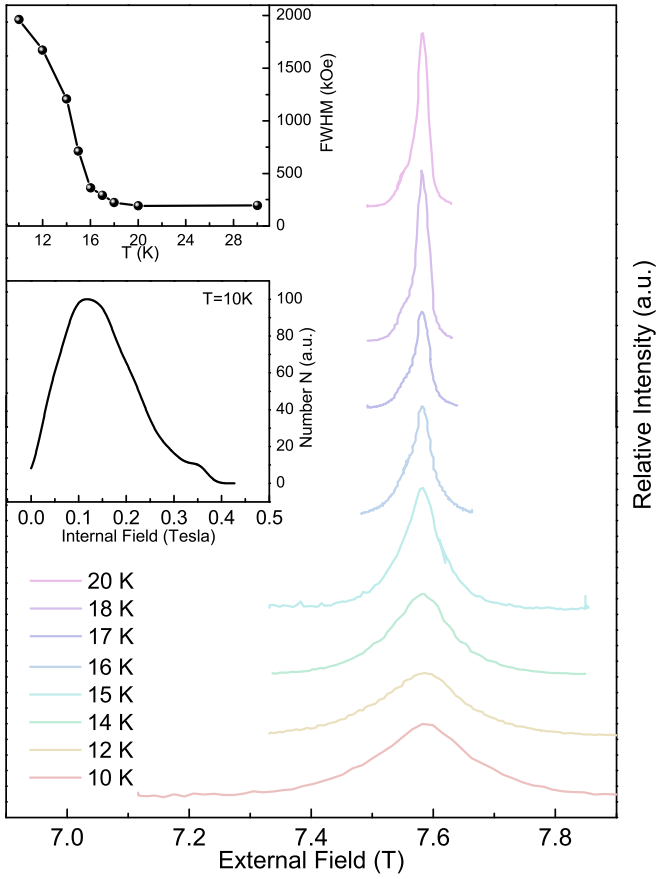

FIG. 3. Temperature dependence of the field-sweep ^{17}O NMR spectrum in $U_{0.15}Np_{0.85}O_2$. Upper inset: Temperature dependence of the full width at half maximum of the ^{17}O spectra. Lower inset: Distribution of the internal field expected from the spectrum broadening at 10 K (solid line).

This evolution is consistent with the presence of a magnetic phase transition, as detected by magnetic susceptibility. There is no remainder of the narrow spectrum from the paramagnetic region, confirming that all the oxygen sites are involved in the bulk phase transition.

C. ^{237}Np Mössbauer spectroscopy

The inset in Fig. 4 presents the Mössbauer spectra acquired at different temperatures on $U_{0.15}Np_{0.85}O_2$. At $T = 40$ K, the spectrum consists of a single peak (no quadrupolar splitting is observed, as expected from cubic symmetry) centered at 8.1 mm/s (relative to the Am metal source), which corresponds to an isomer shift $\delta_{IS} = -5.5$ mm/s relative to the standard $NpAl_2$ absorber. This indicates a Np^{4+} charge state ($5f^3$ electronic configuration) in agreement with XANES [21] results. At $T = 17$ K, the spectrum starts to broaden, suggesting the proximity to a magnetic phase transition. Below this temperature, a magnetically split pattern is observed, indicating the presence of ordered magnetic moments carried by neptunium atoms. As it has been previously observed for other $U_{1-x}Np_xO_2$ compounds, the spectrum is broad and unresolved and has been fitted using the Wegener model of relaxation of the

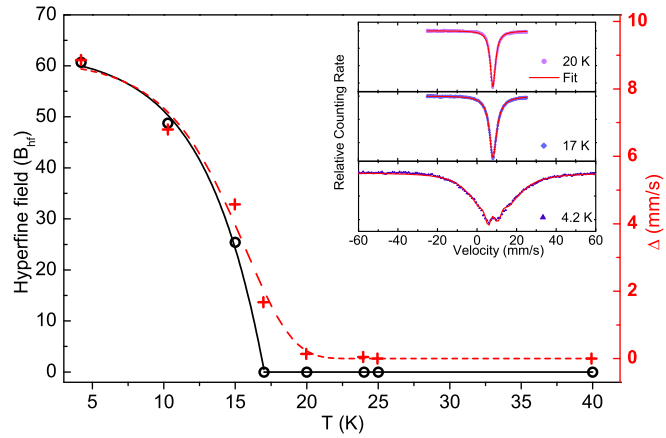

FIG. 4. Temperature dependence of the hyperfine field (B_{hf}) at the ^{237}Np sites and of the line broadening (Δ) of the Mössbauer signal. The inset shows the ^{237}Np Mössbauer spectra recorded above and below the ordering temperature. The red lines represent the best fit to the data obtained using the Wegener model [30,31].

hyperfine magnetic field [30,31]. The magnetic hyperfine field barely reaches 60 T at low temperature, which corresponds to an ordered magnetic moment $\mu_{Np}(4.2\text{ K}) \sim 0.3\mu_B$ ($1\,\mu_B \Leftrightarrow 215$ T [32]). The quadrupolar interaction parameter $e^2qQ = -2.4$ mm/s was also determined and reflects a small induced $5f$ electric-field gradient.

Figure 4 shows the temperature dependence of the hyperfine field B_{hf} and of the broadening parameter Δ, affecting the linewidth of the spectrum in the Wegener model. Both parameters clearly indicate the onset of magnetic ordering around 17 K.

D. Specific heat

In Fig. 5, a magnetic transition is detected at $T = 17.8$ K for $U_{0.15}Np_{0.85}O_2$ on the C_p versus temperature curve. This peak is consistent with the occurrence of magnetic ordering inferred from the other techniques. Furthermore, as the anomaly amplitude slightly decreases with increasing field [33] (inset, Fig. 5), the antiferromagnetic nature of the magnetic structure is confirmed. At 300 K, the heat capacity has a reduced value (64 J mol^{-1} K^{-1}) compared to the empirical Dulong-Petit limit, $C_p = 3nR \sim 75$ J mol^{-1} K^{-1} (with $n = 3$ the number of atoms per formula unit and R the gas constant), depicted by the red dashed line. Such behavior seems to be common in actinide-based oxides [17,44]. The anomaly is smaller in intensity (maximum at 10 kJ mol^{-1} K^{-1}) than the one previously published for NpO_2 [44] (30 kJ mol^{-1} K^{-1}). While the C_p curve of single-crystal $U_{0.75}Np_{0.25}O_2$ previously published showed the presence of additional anomalies, nothing is visible using the present C_p vs T representation (Fig. 5).

IV. DISCUSSION

All the different analytical techniques applied to characterize this neptunium-rich mixed oxide agree on the onset of antiferromagnetic ordering at $T_N \sim 17$ K. Nevertheless, they all pick up a specific behavior.

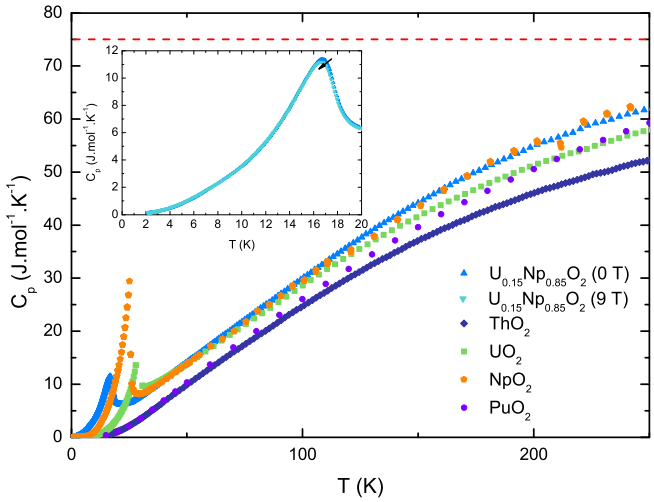

FIG. 5. Heat capacity C_p of $U_{0.15}Np_{0.85}O_2$, ThO_2, UO_2 [54], NpO_2 [44], and $^{242}PuO_2$ [55]. Note that the magnetic peak for UO_2 has been truncated. The Dulong-Petit limit is represented by the red dashed line. The inset shows the magnetic transition peak and the data acquired at 9 and 0 T. The arrow underlines the slight decrease of the magnetic peak when increasing the magnetic field.

A. Magnetic behavior probed by ^{17}O and ^{237}Np

While the sudden broadening of the ^{17}O NMR spectra below T_N (Fig. 3) confirms a bulk magnetic ordering, the observed triangular line shape does not resemble the homogeneous antiferromagnetic (AFM) ordering and its characteristic rectangular line shape as in UO_2 [16] for which all the nuclei have the same internal field [34]. It also does not correspond to the characteristic two-peak structure in the antiferro multipolar ordering state of NpO_2 [11] appearing due to longitudinal triple-q quadrupolar order and a lowering of the symmetry from Fm-3m to Pn-3m space group without any structural distortion [10,12,35]. Our line broadening (Fig. 3) being of comparable magnitude to NpO_2 [11], the appearance of such two-peaks structure should be easily visible. Nonetheless, contrary to NpO_2, for which only one peak (ONp_4 units) was identified by high-resolution NMR [21], for the present solid solution four peaks were detected (ONp_4,OU_1Np_3,OU_2Np_2, and OU_3Np_1 units). The resulting line shape is therefore an average of all these species and the two expected O peaks (which probably occur for each unit) might overlap. In the literature [36,37], such triangular line shape was attributed to incommensurate spin-density wave states where the internal field is distributed due to a modulation of the spin amplitude. However, considering the ac susceptibility which is sensitive to this type of magnetic ordering (variation of T_N with ac susceptibility's frequency), this hypothesis can be rejected as there is no frequency dependency. This type of line shape was also observed in the ordered state of AmO_2 [38] and $NiGa_2S_4$ [39] and it has been suggested that the self-radiation damage from the α decay of Am nuclei leads the magnetic ordering to be in short range in the former, and a geometrical frustration stabilizes the low-temperature spin-disordered state in the latter. In our case though, this triangular line shape definitely indicates that the internal field is largely distributed at the oxygen sites. A clear proof is expressed by the histogram in Fig. 3(b) presenting the internal fields at 10 K and showing that they are distributed from zero to a finite value (~0.4 T) [40].

Despite the large Np substitution, the Mössbauer spectrum still shows the presence of a hyperfine splitting characteristic of magnetic dipole order at the Np site ($\mu_{Np} \sim 0.3\mu_B$) while it is not the case anymore in pure NpO_2 [8,18] ($\mu_{Np} < 0.01\mu_B$). Therefore, these results indicate the persistence of magnetic dipole order in $U_{0.15}Np_{0.85}O_2$. It should be further noted that even a small local distortion, by the substitution, from the cubic symmetry around actinide ions lifts the degeneracy of the crystal-field ground state of $5f$ electrons, which is the Γ_5 triplet for U^{4+} in UO_2 and the Γ_8 quartet for Np^{4+} in NpO_2. In particular, the splitting of the Γ_8 quartet ground state into two Kramers' doublets could lead to the rapid emergence of a magnetic dipole contribution, even in the presence of multipolar interactions.

B. Specific heat data for $U_{0.15}Np_{0.85}O_2$ and comparison to NpO_2

Even though the specific heat results confirm and complement the conclusions drawn from other techniques by detecting the anomaly at ~17 K, we found it intriguing that C_p did not vanish at very low temperature. The presence of a Sommerfeld coefficient (γ), usually attributed to the electronic contribution in metals, has to be excluded here, since for actinide oxides-based material such as UO_2 and NpO_2 no γ was reported. This statement is only reinforced as the previously published C_p of $U_{0.75}Np_{0.25}O_2$ did reach zero at such temperatures [17]. This behavior can be better visualized by plotting C_p/T against T in Fig. 6. As this composition is located in the Np-rich side of the $U_{1-x}Np_xO_2$ diagram and due to NpO_2's peculiar magnetic ordering, we found it relevant to compare (Fig. 6) our present data with the C_p of NpO_2 previously published [41–44]. By using the C_p/T representation for the dioxide, one clearly notices the presence of an upturn at very low temperatures which is not visible on the C_p curve (Fig. 6).

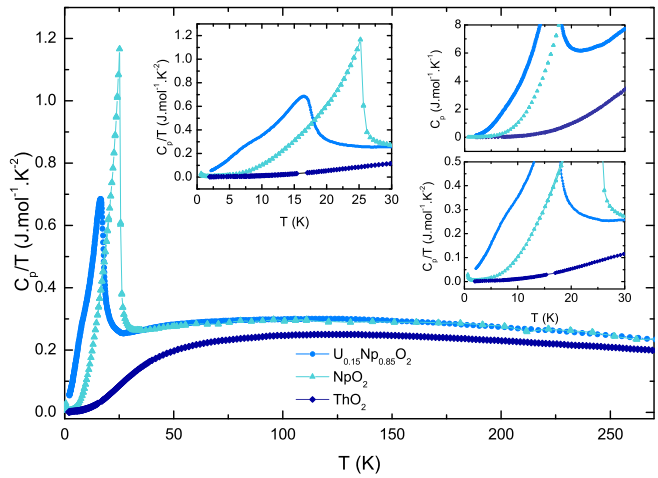

FIG. 6. Plot of C_p/T against T for $U_{0.15}Np_{0.85}O_2$, NpO_2, and ThO_2 at 0 T. The main inset shows the C_p/T curves in the magnetic transition region. The two other insets present a zoom on the C_p and C_p/T curves at low temperature enlightening the differences detected using these two representations (see text).

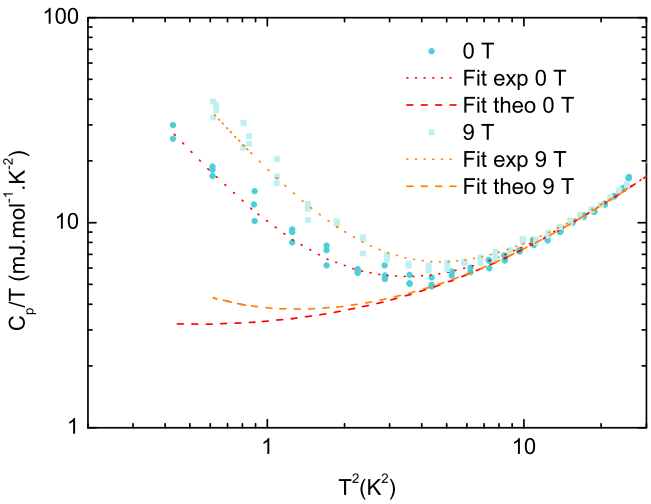

FIG. 7. Zoom on the upturn observed at very low temperatures on the C_p/T curve acquired on the NpO_2 sample at two different magnetic fields. "Fit theo" corresponds to the fit obtained from the Mössbauer parameters and "Fit exp" to obtain the best match with the experimental data (see text for more details).

The most common explanation for this behavior is a splitting of the nuclear ground-state level of the ^{237}Np nuclei (nuclear moment $\mu_I = 3.14\mu_N$ and nuclear spin $I = 5/2$) due to the hyperfine interaction, as previously reported in several Np-based materials [45,46]. In Fig. 7, we show a closer look at the C_p/T curve in the low-temperature range highlighting the upturn. The low-temperature experimental data were fitted using the following equation:

$$C_p/T = \gamma + \beta T^2 + C_2/T^3.$$

The γ and the temperature-dependent Debye term (β) values were obtained by fitting the linear part of C_p/T vs T^2 as $C_p/T = \gamma + \beta T^2$, whereas C_2 can be calculated using either the magnetic hyperfine field or the quadrupole coupling constant inferred from Mössbauer spectroscopy. By fitting the broadening of the zero-field line with decreasing temperature, a quadrupole coupling constant of $e^2qQ = 5.1$ mm/s and an effective magnetic field $B_{hf} = 4.6$ T were previously determined in the ordered phase [8]. In the former case we obtain $C_2 = 6.868 \times 10^{-5}$ J K^{-1} mol^{-1} and in the latter $C_2 = 3.75 \times 10^{-5}$ J K^{-1} mol^{-1} (Fig. 7), whereas a good fit of the low-temperature specific heat upturn can only be obtained using a C_2 value two orders of magnitude larger (corresponding to $B_{hf} \sim 50\,T$ or $e^2qQ \sim 70$mm/s).

In an attempt to clarify this discrepancy, we have also calculated the expected hyperfine splitting of the electronic ground state in the multipolar-ordered phase of NpO_2. Since no ordered magnetic dipole is present in zero field [13] B_{hf} is nil. The lattice contribution to the quadrupole coupling constant is also expected to be negligible, because no distortion is observed below the transition temperature. This leaves the electronic contribution arising from the antiferroquadrupolar order, which can be estimated using the $|\Gamma_5\rangle$ ground-state wave function [47], to calculate $\langle\Gamma_5|3J_z^2|\Gamma_5\rangle - J(J+1) = 7.2$ and the proportionality constant for Np^{4+} reported in Ref. [48] to obtain $e^2qQ = 6.7$ mm/s. We have also considered the possible occurrence of a pseudoquadrupolar hyperfine splitting due to interlevel interaction [49]. To do so, it was necessary to diagonalize the hyperfine coupling Hamiltonian $H_{hf} = A\mathbf{JI}$ over the states which belong to the lowest-energy Γ_8 quartet, considering the energy splittings obtained by inelastic neutron scattering [14] and the coupling constant A, estimated for Np^{4+} [50]. However, this contribution turns out to be not significant, since we obtained an upper bound $e^2qQ \sim 0.3$ mm/s. We can conclude that the hyperfine splitting calculated for NpO_2 is in quantitative agreement with the Mössbauer results, and at least one order of magnitude too small to reproduce the low-temperature specific heat upturn reported in this work, which therefore cannot be purely nuclear in nature. Also, this upturn cannot be due to a Schottky anomaly (electronic), as previously reported [44]. This observation could be linked with the presently observed nonvanishing C_p/T in our $U_{0.15}Np_{0.85}O_2$ sample. We did also verify and confirm that no Schottky anomaly was detected in our mixed-oxide sample. Indeed, we calculated a Schottky peak for two states with the same degeneracy split by a gap of 17 K (value so that the maximum is around 7 K) and, in the ordered phase, similar to that of pure NpO_2 it is really difficult to justify a two-doublet structure.

In addition to this peculiar low-temperature behavior ($C_p \neq 0$), a closer look at the main anomaly detected at 17 K (and also visible with the other techniques) unravels an additional small anomaly at around 7 K (Fig. 6). The presence of an impurity to account for this peak at 7 K has to be excluded if one considers the phase diagram suggested by Wilkins *et al.* [17]. Additionally, such extra anomalies were previously reported for $U_{0.75}Np_{0.25}O_2$ [17], while both NpO_2 and UO_2 present a single peak at 25.7 and 30.8 K, respectively. Systems which present both AFM and AFQ ordering such as DyB_2C_2 [51] or CeB_6 [52] also present an additional anomaly on their C_p curve at a temperature higher than the Néel temperature and not detected by magnetic susceptibility measurements. In the present case, however, the two anomalies cannot indicate the consecutive occurrence of AFM and AFQ ordering. This is because the stabilization of magnetic order at 17 K isolates a singlet ground state, precluding any further phase transition at lower temperatures [13]. Indeed, for this specific series (UO_2, NpO_2, and $U_{0.75}Np_{0.25}O_2$) it was shown that the primary order parameter is the magnetic one, the quadrupolar order following as secondary order parameter [53].

Finally, we calculated the magnetic entropy by integrating the magnetic specific heat, $S_{magn} = \int \frac{C_{magn}}{T} dT$, and plotted the curve in Fig. 8. In order to estimate the magnetic contribution, $C_{magn}(T) = C_p(T) - C_{phonon}(T)$, the specific heat of the nonmagnetic isostructural compound ThO_2 (Fig. 6) was used to account for the phonon contribution, $C_{phonon}(T) \approx C_p(T)^{ThO_2}$. Our approach is similar to the one done previously when calculating the magnetic entropy for UO_2 [54], NpO_2 [14], and PuO_2 [55]. Especially, our C_p curve is very similar, for T above 40 K (i.e., above the magnetic anomaly), to that of NpO_2 (Fig. 5), for which ThO_2 was used to account for the phonon contribution [44]. It is nonetheless worth mentioning that there is a divergence between the C_p curves of ThO_2 and the other oxides (Fig. 5).

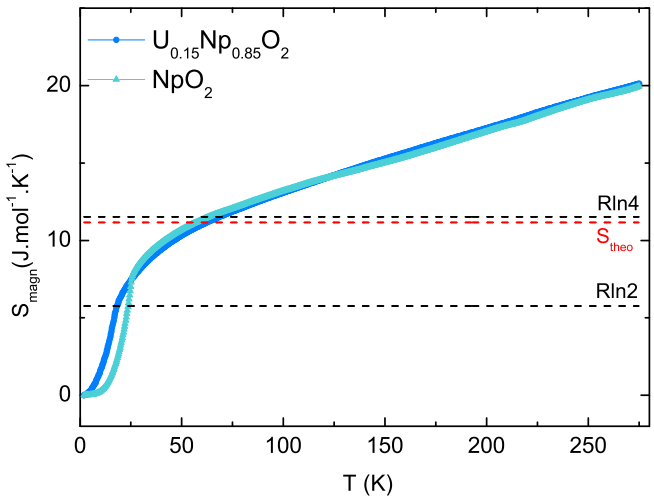

FIG. 8. Temperature dependence of the magnetic entropy S_{magn} of $U_{0.15}Np_{0.85}O_2$ compared to NpO_2. The value S_{theo} (red dashed line) corresponds to the theoretical value R [0.15ln(4)+0.85ln(3)] as suggested by Wilkins *et al.* [17].

We determined $S_{magn} = 5.2$ J mol^{-1} K^{-1} at $T_N = 17$ K for $U_{0.15}Np_{0.85}O_2$ and $S_{magn} = 6.7$ J mol^{-1} K^{-1} at $T_N = 25.7$ K for NpO_2 (in agreement with previous results from Ref. [44]). At this temperature, the value of the theoretical S_{magn} should be equal to $S_{magn}{}^{theo} = R[0.85\ln(4) + 0.15\ln(3)] \sim 11.2$ J mol^{-1} K^{-1} as defined by Wilkins *et al.* [17]. Instead, the value obtained experimentally is close to $R\ln 2 \sim 5.76$ J mol^{-1} K^{-1} corresponding to a doublet ground state. This S_{magn} deficiency at the magnetic transition temperature seems to be characteristic of this series of actinide dioxides [3,41]. Indeed, for NpO_2, it was found $S_{magn} = 6.7$ J mol^{-1} K^{-1}, instead of $R\ln 4 \sim 11.53$ J mol^{-1} K^{-1} (i.e., quartet ground state) [44]. For UO_2, due to the first-order character of the magnetic peak, only an estimation of $S_{magn} = 6.3$ J mol^{-1} K^{-1} was given [54,56]. This value is again lower than the $R\ln 3 \sim 9.13$ J mol^{-1} K^{-1} expected for a triplet ground state, confirming the trend observed for the actinide oxides series. These reduced entropy values were explained by the presence of dynamical Jahn-Teller phenomena [3,9,17] in pure actinide dioxides and could therefore also occur in the present sample. It is worth mentioning that due to this large entropy change, the presence of a Schottky anomaly can also be ruled out.

C. $U_{0.15}Np_{0.85}O_2$ and the other solid solutions

We provide an overview on the Np-rich part of the $U_{1-x}Np_xO_2$ magnetic phase diagram, by comparing in Fig. 9 the present results with those acquired for $x = 0.75$ [18], 0.95, and 1 [41]. In this range, there is a continuous increase of T_{ord}, up to 25.1 K in NpO_2. Even though this behavior was mentioned by Wilkins *et al.* [3], it seems to be more rapid than expected, as a temperature of ∼13 K had been extrapolated for $x = 0.8$. From $x = 0.75$ [20] to $x = 0.85$ and 0.95 the effective moment decreases, before increasing again for $x = 1$. All these values are reduced compared to the free-ion Np^{4+} ($\mu_{eff} = 3.62\,\mu_B$ in Russell-Saunders coupling)

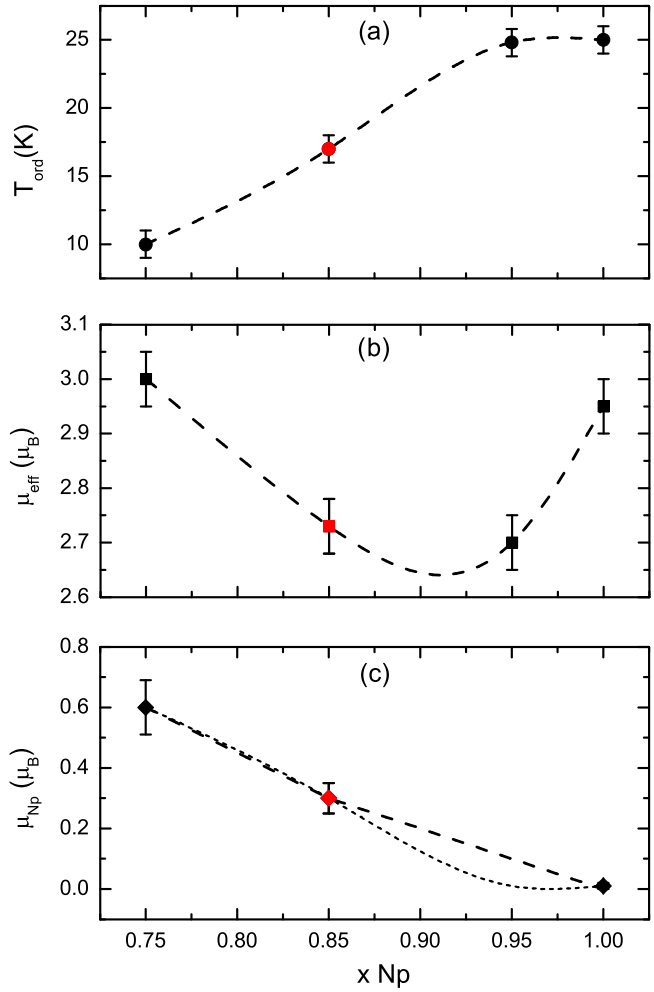

FIG. 9. Variation of (a) the ordered temperature (T_{ord}), (b) the effective moment (μ_{eff}), and (c) the Np ordered moment (μ_{Np}) for the Np-rich $U_{1-x}Np_xO_2$ solid solutions. The dashed lines are obtained for (a) and (b) using a curve interpolation and for (c) a linear interpolation. For (c), the second fit was determined using a curve interpolation and considering that the μ_{Np} was 0 for $x = 0.95$.

due to Jahn-Teller effect. Similar important reduction of the μ_{eff} was detected in the $U_{1-x}Pu_xO_2$ series for low Pu content [57]; the authors attributed that behavior to Jahn-Teller interaction reaching a maximum. Finally, the ordered moment μ_{Np} continuously decreases through the considered range of composition and becomes smaller by a factor of 2 from $x = 0.75$ to 0.85. As the Np ordered moment for $x = 0.95$ is not available in the literature, we fitted the data considering first a linear interpolation (dashed line). Nevertheless, due to the very similar T_{ord} between $x = 1$ and 0.95, we also used an interpolation considering that μ_{Np} is nil for this latter composition.

In summary, considering the persistence of the dipolar order ($\mu_{Np} = 0.3\mu_B$) and the peculiar NMR line shape, we propose that $U_{0.15}Np_{0.85}O_2$ belongs to a third region which is outside of the frustrated magnetic region described by Wilkins *et al.* [3] (from $0.3 < x < 0.8$) and not yet in the pure AFO-L/AFQ-L region as for NpO_2. We cannot clearly infer the presence of antiferroquadrupolar order even though it is expected to

dominate over U-U and U-Np dipolar interactions at such high Np content. A clear answer will only be possible using resonant x-ray scattering or single-crystal ^{17}O NMR techniques.

V. CONCLUSIONS

This study of $U_{0.15}Np_{0.85}O_2$ using several analytical methods points out a region in the complex $U_{1-x}Np_xO_2$ magnetic phase diagram. Indeed, the different techniques all agree on an ordering at $T_N \sim 17$ K but the presence of pure AFM ordering has to be excluded. Magnetization curves reveal the stable character of the antiferromagnetic order in large applied magnetic fields, indicating robust interactions. ^{237}Np Mössbauer spectroscopy shows the presence of a hyperfine splitting due to small but non-negligible magnetic dipole order at the Np site. ^{17}O NMR results show that the internal field at oxygen nuclear positions is largely distributed, suggesting that the ordered moments on the actinide sites is also variable. The interpretation of the specific line shape of the NMR spectrum below T_N as due to a spin-glass effect was ruled out by ac magnetic susceptibility, meaning that the most plausible explanation for the observed line shape is a static magnetic moment distribution. Specific heat results show the presence of a Sommerfeld-like coefficient which was not observed in other dioxides. This anomaly in C_p might be linked with the upturn detected at very low temperature by plotting the C_p/T versus T curve for the pure dioxide NpO_2. Unfortunately, neither the experimental fit deduced from Mössbauer parameters nor the calculated hyperfine splitting of the electronic ground state in the multipolar-ordered phase could explain this behavior in NpO_2. From specific heat data, we also infer the magnetic entropy of $U_{0.15}Np_{0.85}O_2$, which is found smaller than the expected theoretical value but consistent with the reduced values also observed in the end members UO_2 and NpO_2. Such behavior was previously attributed to Jahn-Teller distortions.

ACKNOWLEDGMENTS

The authors thank Jacobus Boshoven, Sarah Noury, and Antony Guiot for the sample's synthesis, Daniel Bouëxière for the XRD analysis, Chris Selfslag for the technical support with the NMR, Anna Smith for her help with the sample preparation for the specific heat analysis, and Joseph Somers for the fruitful discussions.

[1] F. Lebreton, D. Prieur, D. Horlait, T. Delahaye, A. Jankowiak, C. Léorier, F. Jorion, E. Gavilan, and F. Desmoulière, J. Nucl. Mater. **438**, 99 (2013).
[2] A. Fernandez, J. McGinley, J. Somers, and M. Walter, J. Nucl. Mater. **392**, 133 (2009).
[3] S. B. Wilkins, R. Caciuffo, C. Detlefs, J. Rebizant, E. Colineau, F. Wastin, and G. H. Lander, Phys. Rev. B **73**, 060406(R) (2006).
[4] A. Boeuf, R. Caciuffo, J. M. Fournier, L. Manes, J. Rebizant, F. Rustichelli, J. C. Spirlet, and A. Wright, Phys. Status Solidi A **79**, K1 (1983).
[5] A. Delapalme, M. Forte, J. M. Fournier, J. Rebizant, and J. C. Spirlet, Physica B **102**, 171 (1980).
[6] B. D. Dunlap, G. M. Kalvius, D. J. Lam, and M. B. Brodsky, J. Phys. Chem. Solids **29**, 1365 (1968).
[7] J. M. Friedt, Radiochim. Acta. **32**, 105 (1983).
[8] J. M. Friedt, F. J. Litterst, and J. Rebizant, Phys. Rev. B **32**, 257 (1985).
[9] P. Santini and G. Amoretti, Phys. Rev. Lett. **85**, 2188 (2000).
[10] J. A. Paixao, C. Detlefs, M. J. Longfield, R. Caciuffo, P. Santini, N. Bernhoeft, J. Rebizant, and G. H. Lander, Phys. Rev. Lett. **89**, 187202 (2002).
[11] Y. Tokunaga, Y. Homma, S. Kambe, D. Aoki, H. Sakai, E. Yamamoto, A. Nakamura, Y. Shiokawa, R. E. Walstedt, and H. Yasuoka, Phys. Rev. Lett. **94**, 137209 (2005).
[12] Y. Tokunaga, D. Aoki, Y. Homma, S. Kambe, H. Sakai, S. Ikeda, T. Fujimoto, R. E. Walstedt, H. Yasuoka, E. Yamamoto, A. Nakamura, and Y. Shiokawa, Phys. Rev. Lett. **97**, 257601 (2006).
[13] P. Santini, S. Carretta, N. Magnani, G. Amoretti, and R. Caciuffo, Phys. Rev. Lett. **97**, 207203 (2006).
[14] N. Magnani, S. Carretta, R. Caciuffo, P. Santini, G. Amoretti, A. Hiess, J. Rebizant, and G. H. Lander, Phys. Rev. B **78**, 104425 (2008).
[15] P. Burlet, J. Rossat-Mignod, S. Quezel, O. Vogt, J. C. Spirlet, and J. Rebizant, J. Less-Common Met. **121**, 121 (1986).
[16] K. Ikushima, S. Tsutsui, Y. Haga, H. Yasuoka, R. E. Walstedt, N. M. Masaki, A. Nakamura, S. Nasu, and Y. Ōnuki, Phys. Rev. B **63**, 104404 (2001).
[17] S. B. Wilkins, J. A. Paixão, R. Caciuffo, P. Javorsky, F. Wastin, J. Rebizant, C. Detlefs, N. Bernhoeft, P. Santini, and G. H. Lander, Phys. Rev. B **70**, 214402 (2004).
[18] A. Tabuteau, J. Jové, M. Pagès, C. H. de Novion, and J. Gal, Solid State Commun. **50**, 357 (1984).
[19] A. Boeuf, R. Caciuffo, M. Pagès, J. Rebizant, F. Rustichelli, and A. Tabuteau, Europhys. Lett. **3**, 221 (1987).
[20] A. Tabuteau, M. Pagès, A. Bœuf, J. Rebizant, L. Manes, R. Caciuffo, and F. Rustichelli, J. Phys. Lett. **45**, 373 (1984).
[21] L. Martel, J.-F. Vigier, D. Prieur, S. Nourry, A. Guiot, K. Dardenne, J. Boshoven, and J. Somers, J. Phys. Chem. C **118**, 27640 (2014).
[22] B. C. Frazer, G. Shlrane, D. E. Cox, and C. E. Olson, Phys. Rev. **140**, A1448 (1965).
[23] W. Huang, M. Schopfer, C. Zhang, R. C. Howell, L. Todaro, B. A. Gee, L. C. Francesconi, and T. Polenova, J. Am. Chem. Soc. **130**, 481 (2008).
[24] S. L. Poulsen, V. Kocaba, G. L. Saoût, H. J. Jakobsen, K. L. Scrivener, and J. Skibsted, Solid State Nucl. Magn. Reson. **36**, 32 (2009).
[25] A. Ferreira, D. Ananias, L. D. Carlos, C. M. Morais, and J. Rocha, J. Am. Chem. Soc. **125**, 14573 (2003).
[26] M. B. Ley, D. B. Ravnsbæk, Y. Filinchuk, Y. S. Lee, R. Janot, Y. W. Cho, J. Skibsted, and T. R. Jensen, Chem. Mater. **24**, 1654 (2012).
[27] S. Ivanova, E. Zhecheva, R. Stoyanova, D. Nihtianova, S. Wegner, P. Tzvetkova, and S. Simova, J. Phys. Chem. C **115**, 25170 (2011).
[28] Y. Tokunaga, T. Nishi, S. Kambe, M. Nakada, Y. Homma, H. Sakai, and H. Chudo, J. Phys. Soc. Jpn. **80**, SA110 (2011).

[29] L. Martel, N. Magnani, J.-F. Vigier, J. Boshoven, C. Selfslag, I. Farnan, J.-C. Griveau, J. Somers, and T. Fanghänel, Inorg. Chem. **53**, 6928 (2014).
[30] H. Wegener, Z. Phys. **186**, 498 (1965).
[31] J. Gal, Z. Hadari, U. Atzmony, E.R. Bauminger, I. Nowik, and S. Ofer, Phys. Rev. B **8**, 1901 (1973).
[32] B. D. Dunlap and G. H. Lander, Phys. Rev. Lett. **33**, 1046 (1974).
[33] J. G. Sereni, in *Encyclopedia of Materials: Science and Technology Vol. 5*, Magnetic Systems: Specific Heat (Elsevier, Oxford, 2001), pp. 4986–4993.
[34] Y. Ideta, Y. Kawasaki, Y. Kishimoto, T. Ohno, Y. Michihiro, Z. He, Y. Ueda, and M. Itoh, Phys. Rev. B **86**, 094433 (2012).
[35] D. Mannix, G. H. Lander, J. Rebizant, R. Caciuffo, N. Bernhoeft, E. Lidström, and C. Vettier, Phys. Rev. B **60**, 15187 (1999).
[36] M. Kontani, T. Hioki, and Y. Masuda, J. Phys. Soc. Jpn. **39**, 672 (1975).
[37] H. Sakurai, N. Tsuboi, M. Kato, K. Yoshimura, K. Kosuge, A. Mitsuda, H. Mitamura, and T. Goto, Phys. Rev. B **66**, 024428 (2002).
[38] Y. Tokunaga, T. Nishi, M. Nakada, A. Itoh, H. Sakai, S. Kambe, Y. Homma, F. Honda, D. Aoki, and R. E. Walstedt, Phys. Rev. B **89**, 214416 (2014).
[39] H. Takeya, K. Ishida, K. Kitagawa, Y. Ihara, K. Onuma, Y. Maeno, Y. Nambu, S. Nakatsuji, D. E. MacLaughlin, A. Koda, and R. Kadono, Phys. Rev. B **77**, 054429 (2008).
[40] Y. Tokunaga, H. Sakai, S. Kambe, H. Chudo, M. Osaka, S. Miwa, T. Nishi, M. Nakada, A. Itoh, and Y. Homma, MRS Proc. **1444**, mrss12-1444 (2012).
[41] D. W. Osborne and E. F. Westrum, Jr., J. Chem. Phys. **21**, 1884 (1953).
[42] P. Erdös, G. Solt, Z. Zolnierek, A. Blaise, and J. M. Fournier, Physica B **102**, 164 (1980).
[43] J. W. Ross and D. J. Lam, J. Appl. Phys. **38**, 1451 (1967).
[44] N. Magnani, P. Santini, G. Amoretti, R. Caciuffo, P. Javorský, F. Wastin, J. Rebizant, and G. H. Lander, Physica B **359-361**, 1087 (2005).
[45] V. H. Tran, J.-C. Griveau, R. Eloirdi, and E. Colineau, Phys. Rev. B **89**, 054424 (2014).
[46] A. Hen, E. Colineau, R. Eloirdi, J.-C. Griveau, N. Magnani, F. Wilhelm, A. Rogalev, J.-P. Sanchez, A. B. Shick, I. Halevy, I. Orion, and R. Caciuffo, Phys. Rev. B **90**, 054408 (2014).
[47] S. Di Matteo, N. Magnani, F. Wastin, J. Rebizant, and R. Caciuffo, J. Alloys Compd. **444-445**, 278 (2007).
[48] G. Amoretti, M. Bogé, J. M. Fournier, A. Blaise, and A. Wojakowski, J. Magn. Magn. Mater. **66**, 236 (1987).
[49] N. I. Agladze, E. A. Vinogradov, and M. N. Popova, Sov. Phys. JETP **64**, 716 (1986).
[50] N. Edelstein, W. Kolbe, and J. E. Bray, Phys. Rev. B **21**, 338 (1980).
[51] H. Yamauchi, H. Onodera, K. Ohoyama, T. Onimaru, M. Kosaka, M. Ohashi, and Y. Yamaguchi, J. Phys. Soc. Jpn. **68**, 2057 (1999).
[52] T. Fujita, M. Suzuki, T. Komatsubara, S. Kunii, T. Kasuya, and T. Ohtsuka, Solid State Commun. **35**, 569 (1980).
[53] P. Santini, S. Carretta, G. Amoretti, R. Caciuffo, N. Magnani, and G. H. Lander, Rev. Mod. Phys. **81**, 807 (2009).
[54] J. J. Huntzicker and E. F. Westrum, Jr., J. Chem. Thermodyn. **3**, 61 (1971).
[55] H. E. Flotow, D. W. Osborne, S. M. Fried, and J. G. Malm, J. Chem. Phys. **65**, 1124 (1976).
[56] G. Dolling, R. A. Cowley, and A. D. B. Woods, Can. J. Phys. **43**, 1397 (1965).
[57] D. Kolberg, F. Wastin, J. Rebizant, P. Boulet, G. H. Lander, and J. Schoenes, Phys. Rev. B **66**, 214418 (2002).